JACS
JOURNAL OF THE AMERICAN CHEMICAL SOCIETY

Subscriber access provided by American Chemical Society

Article

Electron Density Distributions of Redox Active Mixed Valence Carboxylate Bridged Trinuclear Iron Complexes

Jacob Overgaard, Finn K. Larsen, Birgit Schitt, and Bo B. Iversen

J. Am. Chem. Soc., **2003**, 125 (36), 11088-11099• DOI: 10.1021/ja0346072 • Publication Date (Web): 16 August 2003

Downloaded from http://pubs.acs.org on March 29, 2009

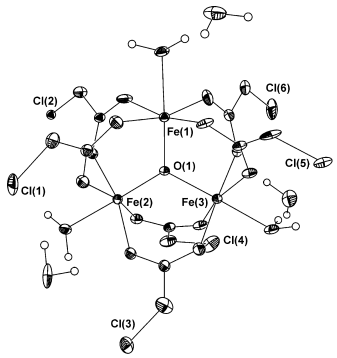

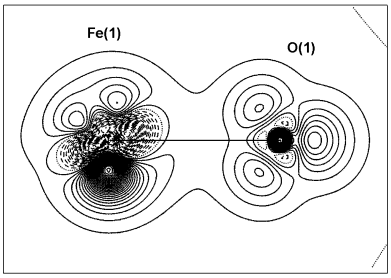

More About This Article

Additional resources and features associated with this article are available within the HTML version:

- Supporting Information
- Links to the 5 articles that cite this article, as of the time of this article download
- Access to high resolution figures
- Links to articles and content related to this article
- Copyright permission to reproduce figures and/or text from this article

View the Full Text HTML

ACS Publications
High quality. High impact.

Journal of the American Chemical Society is published by the American Chemical Society. 1155 Sixteenth Street N.W., Washington, DC 20036

J|A|C|S
ARTICLES
Published on Web 08/16/2003

Electron Density Distributions of Redox Active Mixed Valence Carboxylate Bridged Trinuclear Iron Complexes

Jacob Overgaard,[†] Finn K. Larsen,*[,‡] Birgit Schiøtt,[‡] and Bo B. Iversen*[,‡]

Contribution form the Department of Chemistry, University of Aarhus, Langelandsgade 140, DK-8000 Aarhus, Denmark, School of Chemistry, University of Sydney, Sydney, NSW 2006, Australia

Received February 11, 2003; E-mail: bo@chem.au.dk; kre@chem.au.dk

Abstract: The electron density distributions (EDD) of the redox active mixed valence trinuclear oxo-centered iron carboxylate, $[Fe_3O(CH_2ClCOO)_6(H_2O)_3]\cdot 3H_2O$, **1**, and the oxidized form of **1**, $[Fe_3O(CH_2ClCOO)_6(H_2O)_2(CH_2ClCOO)]\cdot 1H_2O$, **2**, as well as of $[Fe_3O(C(CH_3)_3COO)_6(NC_5H_5)_3]$, **3**, have been determined from accurate single-crystal X-ray diffraction data measured at 100 K (**1**, **2**) and from extensive synchrotron radiation X-ray diffraction data measured at 28 K (**3**). Analysis of the EDDs shows that the central oxygen atom has a very different EDD in the mixed valence complexes (**1** and **3**) compared with the oxidized complex (**2**). Furthermore, in **1** and **3** the chemical bonds between formally identical trivalent Fe atoms and the central oxygen are fundamentally different. This is in direct contrast to the Fe^{III}-(μ^3-O) bonds in the oxidized complex, which are practically identical. Analysis of the d-orbital populations on the metal sites in the three complexes shows that the extra electron density on the Fe^{II} site primarily is distributed in a d(yz) orbital (*z*-axis toward the central oxygen, *y*-axis perpendicular to the Fe_3O-plane). Presence of extra charge in the d(yz) orbital correlates with a decrease in the d(xy) population, i.e., with a depletion of charge in the equatorial region of coordination to carboxylate oxygen. The d(xy) charge depletion appears to be of importance for determining the active versus trapped Fe^{III} site, and the equatorial ligands therefore have a considerable influence on the ET process. Bader topological analysis of the EDDs corroborates the conclusions drawn from the orbital population analysis, but it also provides additional knowledge about the chemical bonding in the structures. For comparison with the X-ray results, theoretical calculations were carried out for **3** in the experimental geometry. The present information about ET processes in trinuclear oxo-centered iron complexes cannot be deduced from analysis of the molecular structures (i.e., bond lengths and angles), and thus it is demonstrated that X-ray charge density analysis is able to reveal subtle new features of significant physical and chemical importance on complex molecular systems.

Introduction

Redox active mixed valence (MV) polynuclear transition metal centers are involved in many of natures electron transfer (ET) processes.[1] In enzymes, the transition metal atoms at the active sites are often linked by oxo, hydroxy or water bridges, and a large number of studies have attempted to synthesize and analyze model complexes with similar properties as possessed by proteins.[2] Besides the obvious importance for basic research, studies of model complexes also aim at developing catalysts, which can perform the functions of enzymes in controlled environments suitable for industrial applications. The trinuclear oxo-centered carboxylate-bridged iron complexes (TOCIs), $[Fe^{III}_2Fe^{II}O(O_2CR)_6L_3]\cdot nS$,[3] constitute one of the most studied classes of MV model compounds due to their relative simplicity, their potential use as oxidation catalysts and their many interesting physical properties.[4]

The temperature dependence of the ET has been studied in a number of MV TOCIs with multi-temperature ^{57}Fe Mössbauer spectroscopy,[5] a technique which locally probes the valence state of each iron atom on a time scale of $10^{-7}-10^{-8}$ s. However, the results obtained from Mössbauer spectroscopy[5j,m] on the onset temperature and the nature of ET has in some cases been disputed by X-ray crystallographic results.[6] These contradictions may originate in the differences in time scales between the two experimental methods, and they emphasize the need for multi-temperature X-ray crystallographic analysis to assist in pinpointing the factors affecting the ET in MV complexes. However, such investigations have only been carried out for a few trinuclear MV systems, where the onset of ET has been correlated with order−disorder transitions in the solvent or ligand molecules.[6]

The concept of MV is widely used in chemistry, but simple chemical electron counting rules are not an accurate representation of the actual electron density distribution (EDD) of MV

[†] School of Chemistry, University of Sydney.
[‡] Department of Chemistry, University of Aarhus.

(1) Lippard, S. J. *Angew. Chem.* **1988**, *100*, 353−370; Angew. *Chem. Int. Ed. Engl.* **1988**, *27*, 344−361.
(2) Limburg, J.; Vrettos, J. S.; Liable-Sands, L. M.; Rheingold, A. L.; Crabtree, R. H.; Brudvig, G. W. *Science* **1999**, *283*, 1524−1527.
(3) RCOO designates substituted carboxylate bridges, L terminal ligands and S solvates.
(4) Cannon, R. D.; White, R. P. *Prog. Inorg. Chem.* **1988**, *36*, 195−297.

10.1021/ja0346072 CCC: $25.00 **© 2003 American Chemical Society**

molecules. Because the EDD is a proper quantum mechanical observable, knowledge of the EDD of MV systems can potentially improve our understanding of active enzymes and therefore also our predictive power for their properties.[7] The EDD of molecular systems can either be obtained from quantum mechanical calculations or estimated experimentally from accurate X-ray diffraction data.[8] Even though great advances have occurred in computational chemistry, it is still very difficult to theoretically estimate accurate EDDs of low symmetry systems containing hundreds of atoms of which several may be open shell transition metals. Contrary to this, the experimental X-ray technique is less affected by size and symmetry restrictions on the system.[9] Recently this field has been revitalized due to major advances both in the experimental methods and in the interpretation tools. Experimentally, it is the new X-ray area detectors,[10] the availability of intense short wavelength synchrotron radiation,[11] and the development of stable helium cooling devices,[12] which have produced very significant improvements in the data accuracy. However, a restriction on the applicability of X-ray charge density methods in studies of redox active MV complexes is the availability of crystalline systems having a valence trapped configuration and limited structural disorder.

We have previously studied the temperature dependence of the ET in $[Fe_3O(C(CH_3)_3COO)_6(NC_5H_5)_3]$, **3**, for which the 10 K molecular structure is shown in Figure 1c.[6] Compound **3** is in a valence trapped configuration only at very low temperature (<35 K). At higher temperatures, ET takes place between two of the three Fe atoms, leaving the third atom in a trivalent oxidation state at all temperatures (as determined from both variable temperature Mössbauer and X-ray studies). Another example of ET involving only two out of the three iron atoms is compound **1**, $[Fe_3O(CH_2ClCOO)_6(H_2O)_3]\cdot 3H_2O$, Figure 1a, in which the ET onset temperature is approximately 120 K.[5f] In the present paper, we report the experimental EDD of **1** determined from new accurate single-crystal X-ray diffraction data measured at 100 K. The fact that **1** is in the valence trapped state already at 120 K simplifies the experimental conditions since the study can be carried out with a liquid nitrogen cooling device. Furthermore, the excellent crystal quality, the relatively "small" molecular structure and the centrosymmetric crystal

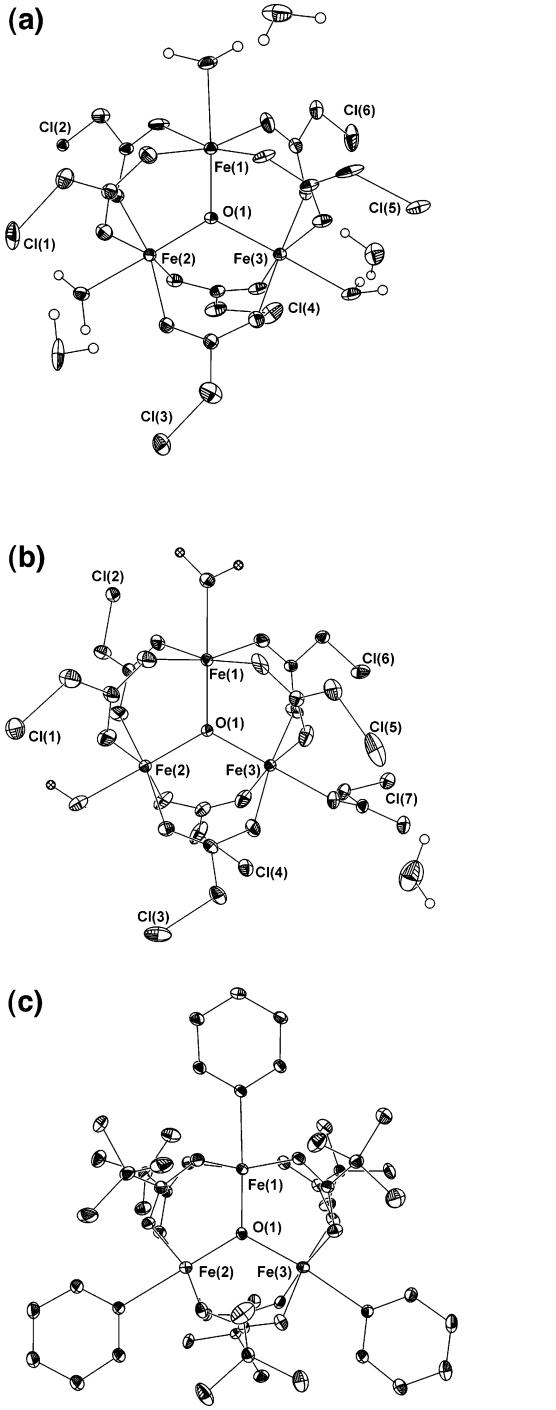

Figure 1. Molecular structures of (a) $[Fe_3O(CH_2ClCOO)_6(H_2O)_3]\cdot 3H_2O$, **1**, (b) $[Fe_3O(CH_2ClCOO)_6(H_2O)_2(CH_2ClCOO)]\cdot 1H_2O$, **2**, and (c) $[Fe_3O(C(CH_3)_3COO)_6(NC_5H_5)_3]$, **3**. Thermal ellipsoids shown at 50% level. All hydrogen atoms (except in the water molecules) are omitted for clarity.

(5) (a) Dziobkowski, C. T.; Wrobleski, J. T.; Brown, D. B. *Inorg. Chem.* **1981**, *20*, 679−684, (b) Oh, S. M.; Hendrickson, D. N.; Hassett, K. L.; Davis, R. E. *J. Am. Chem. Soc.* **1985**, *107*, 8009−8018, (c) Woehler, S. E.; Wittebort, R. J.; Oh, S. E.; Hendrickson, D. N.; Inniss, D.; Strouse, C. E. *J. Am. Chem. Soc.* **1986**, *108*, 2938−2946, (d) Kaneko, Y.; Nakano, M.; Sorai, M.; Jang, H. G.; Hendrickson, D. N. *Inorg. Chem.* **1989**, *28*, 1067−1073, (e) Jang, H. G.; Wittebort, R. J.; Sorai, M.; Kaneko, Y.; Nakano, M.; Hendrickson, D. N. *Inorg. Chem.* **1992**, *31*, 2265−2271, (e) Asamaki, K.; Nakamoto, T.; Kawata, S.; Sano, H.; Katada, M.; Endo, K. *Inorg. Chim. Acta* **1995**, *236*, 155−161, (f) Sato, T.; Ambe, F.; Endo, K.; Katada, M.; Maeda, H.; Nakamoto, T.; Sano, H. *J. Am. Chem. Soc.* **1996**, *118*, 3450−3458, (g) Nakamoto, T.; Yoshida, M.; Kitagawa, S.; Katada, M.; Endo, K.; Sano, H. *Polyhedron* **1996**, *15*, 2131−2139, (h) Nakamoto, T.; Hanaya, M.; Katada, M.; Endo, K.; Kitagawa, S.; Sano, H. *Inorg. Chem.* **1997**, *36*, 4347−4359, (i) Wu, C.-C.; Hunt, S. A.; Gantzel, P. K.; Gütlich, P.; Hendrickson, D. N. *Inorg. Chem.* **1997**, *36*, 4717−4733, (j) Wu, R.; Poyraz, M.; Sowrey, F. E.; Anson, C. E.; Wocadlo, S.; Powell, A. K.; Jayasooriya, U. A.; Cannon, R. D.; Nakamoto, T.; Katada, M.; Sano, H. *Inorg. Chem.* **1998**, *37*, 1913−1921, (k) Nakamoto, T.; Katada, M.; Endo, K.; Sano, H. *Polyhedron* **1998**, *17*, 3507−3514, (l) Nakamoto, T.; Katada, M.; Sano, H. *Inorg. Chim. Acta* **1999**, *291*, 127−135, (m) Manago, M.; Hayami, S.; Yano, Y.; Inoue, K.; Nakata, R.; Ishida, A.; Maeda, Y. *Bull. Chem. Soc. Jpn.* **1999**, *72*, 2229−2234.
(6) Wilson, C.; Iversen, B. B.; Overgaard, J.; Larsen, F. K.; Wu, G.; Palii, S. P.; Timco, G. A.; Gerbeleu, N.V. *J. Am. Chem. Soc.* **2000**, *122*, 11 370−11 379.
(7) R. F. W. Bader, *Atoms in Molecules. A Quantum Theory*; Clarendon Press: Oxford, 1990.
(8) P. Coppens, *X-ray Charge Densities and Chemical Bonding*; Oxford Science Publications: New York, 1997.
(9) Overgaard, J.; Iversen, B. B.; Larsen, F. K.; Palii, S. P.; Timco, G. A.; Gerbeleu, N. V. *Chem. Eur. J.* **2002**, *8*, 2775−2786. In this paper, the experimental electron density of an octanuclear chromium complex with 272 unique atoms (1144 electrons) is presented.
(10) Martin, A.; Pinkerton, A. A. *Acta Crystallogr. Sect. B.* **1998**, *54*, 471−477.
(11) (a) Bolotovsky, R.; White, A. M.; Darovsky, A.; Coppens, P. *J. Synchrotron Radiat.* **1995**, *2*, 181−184; (b) Koritzansky, T.; Flaig, R.; Zobel, D.; Krane, H.-G.; Morgenroth, W.; Luger, P. *Science* **1998**, *279*, 356−358; (c) Iversen, B. B.; Larsen, F. K.; Pinkerton, A.; Martin, A.; Darovsky, A.; Reynolds, P. A. *Acta Crystallogr. Sect. B* **1999**, 55, 363−374.
(12) (a) Larsen, F. K. *Acta Crystallogr. Sect. B.* **1995**, *51*, 468−482. (b) Hardie, M. J.; Kirschbaum, K.; Martin, A.; Pinkerton, A. A. *J. Appl. Crystallogr.* **1998**, *31*, 815−817. (c) Ribaud, L.; Wu, G.; Zhang, Y. G.; Coppens, P. *J. Appl. Crystallogr.* **2001**, *34*, 76−79.

structure make X-ray charge density analysis more feasible. In addition to the study of **1**, we also present the molecular structure and EDD of the oxidized form of **1**, namely $[Fe_3O(CH_2ClCOO)_6(H_2O)_2(CH_2ClCOO)]\cdot 1H_2O$, **2**, Figure 1b. This compound also is suitable for X-ray charge density analysis, and comparison between **1** and **2** makes it possible to directly examine the effects of mixed valence on the trinuclear core. Finally, we have attempted to determine the EDD of **3** in its valence trapped state. Complex **3** contains 133 unique atoms (542 e^-) including three open shell iron atoms in an acentric spacegroup. Taken in combination with the very low temperatures necessary to reach the valence trapped state (<35 K), this EDD study is challenging, and it is made possible only with the use of high-intensity synchrotron radiation and helium based cooling devices.

To compare with the results from the X-ray experiment single point theoretical calculations of **3** in the experimental geometry have been carried out. Theoretical calculations on **1** and **2** are more difficult due to the structural disorder on the chlorine sites. Results are reported for a high spin state of 3 in correspondence with the experimental results. A comprehensive theoretical account of the structure of **3** is beyond the scope of the present paper. The main point here is to show that the experimental density is accurate enough to constrain and validate theoretical results.

Experimental Section

Preparation of $[Fe_3O(CH_2ClCOO)_6(H_2O)_3]\ 3H_2O$. Compound 1. Following ref 5f, a mixture of 28.5 g of chloroacetic acid and 6 g of $FeCl_2\cdot xH_2O$ was dissolved in 75 mL of water by heating. This solution was left to stand in air. With intervals of ~1 week the precipitated solid was redissolved by stirring. After two months, a black solid was isolated by filtration and kept in a closed container.

Preparation of $[Fe_3O(CH_2ClCOO)_6(H_2O)_2(CH_2ClCOO)]\ 1H_2O$. Compound 2. The filtrate from the isolation of **1** was left standing in a covered flask for two months. The dark-yellow precipitate was filtered off and kept in an airtight container.

Preparation of $[Fe_3O(C(CH_3)_3COO)_6(C_5H_5N)_3]$. Compound 3. See ref 6.

Data Collection and Reduction. 1. A black single crystal (0.125 × 0.275 × 0.45 mm^3) was mounted on a few carbon fibers glued to a small piece of copper wire. This arrangement was attached to a brass pin, which was placed on the goniometer head of a Bruker SMART1000 CCD diffractometer at the Department of Chemistry at the University of Aarhus. The crystal temperature was kept at 100(1) K using a liquid nitrogen Oxford Cryocooler fitted on the diffractometer. A combination of ω- and ϕ-scans was used to ensure a good coverage of reciprocal space and produce an accurate empirical absorption correction. During 6 days of data collection, 169 953 reflections were collected and subsequently integrated using SAINT+[13] and they were absorption-corrected with SADABS (T_{max};T_{min}= 1.00; 0.791).[13] The corrected data were averaged with SORTAV[14] resulting in 28 389 unique data with an internal agreement of 2.4%. For further details please refer to Table 1.

2. An orange-red crystal of dimensions 0.175 × 0.20 × 0.25 mm^3 was mounted like **1**. Both ω- and ϕ-scans were employed to collect a total of 147 315 reflections in 6 days. After integration with SAINT+[13] and absorption correction with SADABS,[14] the data were averaged with SORTAV[14] to obtain 24 377 unique reflections with an internal agreement of 2.2% for all averaged data. For further details please refer to Table 1.

Table 1. Crystallographic Details

	1	2	3
formula,weight	$Fe_3Cl_6O_{19}C_{12}H_{24}$ 798.5	$Fe_3Cl_7O_{18}C_{14}H_{20}$ 892	$Fe_3N_3O_{13}C_{45}H_{69}$ 1027.1
space group	$P2_1/n$	$P2_1/c$	$P2_1$
T (K)	100	100	28
a (Å)	13.952(2)	18.382(5)	11.583(1)
b (Å)	14.349(2)	11.360(3)	19.729(1)
c (Å)	14.746(2)	15.050(4)	11.850(1)
β (°)	100.282(3)	108.55(1)	106.527(1)
V (Å^3)	2905(1)	2980	2596(1)
λ (Å)	0.71073	0.71073	0.643
Z	4	4	2
ρ_{calc} (g cm^{-3})	1.826	1.989	1.313
μ (mm^{-1})	2.09	2.14	0.627
T_{max}/T_{min}	1.00; 0.791	1.00; 0.890	no correction
data reduction			
integrated reflections	169 953	147 315	146 326
averaged reflections	161 189	141 383	129 839
discarded reflections	8764	5932	16 487
unique reflections	28 389	24 377	32 567
redundancy	5.7	5.8	4.0
R_{int}	0.025	0.021	0.034
$\sin(\theta)/\lambda_{max}$ (Å^{-1})	1.065	1.026	1.060
refinement on F^2			
N_{par}	988	1069	1098
N_{obs} (σ-cutoff)	15136 (3)	13978 (2)	25606 (3)
$R(F)$, $R(F^2)$	0.020; 0.026	0.023, 0.031	0.034; 0.047
$R_w(F)$, $R_w(F^2)$	0.019, 0,037	0.022, 0.044	0.033, 0.064
goodness of fit	0.72	0.79	1.25

3. A single crystal (0.100 × 0.100 × 0.075 mm^3) mounted on a brass pin using carbon fibers glued to a copper wire was placed directly in the cold finger of a type 201 Displex fitted to a HUBER type 512 four-circle diffractometer. During the measurements an anti-scatter device fitted inside the vacuum enclosure was used to reduce the background radiation and remove parasitic scattering stemming from the vacuum enclosure.[15] A Si(200) monochromator was used to obtain a wavelength of 0.643 Å from the bending magnet at beam line X3A1 at the NSLS, Brookhaven National Laboratory. The diffracted radiation was detected with a Bruker SMART1000 CCD detector mounted on the 2θ arm of the diffractometer, and the subsequent data reduction was performed using the Bruker SMART program package.[13] A ϕ-scan experiment with $\Delta\phi = 0.3°$ was performed with fixed χ- and ω-angles. The CCD-detector was placed at a fixed distance of 4.7 cm from the crystal. Use of eight different settings of the detector in the 2θ-range from 0° to 55° ensured a good coverage of reciprocal space with a maximum resolution of 1.057 Å^{-1}. In this resolution range 146 326 Bragg reflections were integrated with SAINT+[13] and averaged with SORTAV[14] to give 32 567 unique reflections with an internal agreement of 3.4%. Due to the small crystal size and the short synchrotron wavelength, absorption effects were negligible. Some very low order data were missing from the dataset due to the use of the anti scatter device.[16] The data were therefore supplemented with a conventional low-order data set ($\sin\theta/\lambda$ < 0.62 Å^{-1}) measured at a matching temperature (35 K). The small temperature difference between the conventional data (35 K) and the synchrotron data (28 K) is not important at these low temperatures with close to zero point thermal motion. For the conventional data set a crystal of **3** of approximate dimensions 0.38 × 0.31 × 0.24 mm^3 was mounted in an oil film and placed on a nylon fiber. This crystal was cooled to 35(1) K using an Oxford cryosystems open flow He gas cryostat mounted on a Bruker SMART1000 CCD diffractometer at the Department of Chemistry, University of Durham. Data reduction including an empirical absorption correction was carried out with the SMART program package.[13] For further details please refer to Table 1.

(13) Sheldrick, G. S. SAINT+, SADABS, and SHELXL programs included in the Siemens Analytical X-ray Systems. SMART CCD software, 1995.
(14) Blessing, R. H. *J. Appl. Crystallogr.* **1997**, *30*, 421−426 and references therein.
(15) Darovsky, A.; Bolotovsky, R.; Coppens, P. *J. Appl. Crystallogr.* **1994**, *27*, 1039−1040.
(16) Iversen, B. B.; Larsen, F. K.; Pinkerton, A. A.; Martin, A.; Darovsky, A.; Reynolds, P. A. *Acta Crystallogr. Sect. B* **1999**, *55*, 363−374.

Refinement. 1. All non-H atoms were reconstructed from the diffraction data using the direct methods program in SHELX.[13] Some hydrogen atoms were located in a Fourier synthesis, the remaining H atoms were placed on calculated positions (neutron values) and all were refined as 'riding' on the connected atoms.[17] Comparison with the room-temperature structure shows that the crystal is in the valence trapped state.[6] The vibrational description of the chlorine atoms is difficult using only harmonic motion. One chlorine atom is best described with one major and one minor position (with relative weight distribution: 93%, 7%), for another chlorine a reasonable description necessitates two minor positions (93%, 4%, 3%). A third Cl-atom has previously been shown to behave very anisotropically,[5f] and a difference Fourier map in the approximate plane of atomic vibration (see the Supporting Information) strongly indicates that a one site model is not a good description of the density. Instead, a disordered atom with several components of decreasing occupancy as a function of the distance to the center of mass was used. We refined this atom as eight partly occupied chlorine atoms summing to a total of one. Individual isotropic thermal parameters for each component could be refined separately to almost equal values. The final structural model was imported into the program XD,[18] where an initial high order refinement (sin $\theta/\lambda > 0.8$ Å^{-1}) was performed. The resulting structural skeleton (i.e., positions and thermal parameters) was kept fixed in the initial multipole refinements.[19] The data used for this modeling consisted only of data measured more than once, which reduced the number of unique data to 27 129. A sequence of refinements was carried out, in which the complexity of the model was increased stepwise. The final model included hexadecapoles on Fe, octupoles on all other non-H atoms and a set of one monopole and one bond directed dipole for all H attached to C and a similar set for all H in water molecules. Hexadecapoles were observed to be insignificant on O(1), and thus omitted. Local mirror symmetry across the Fe_3O plane was imposed on O(1). Ionic scattering factors[20] were employed for Fe^{3+} and Fe^{2+}. Different radial distributions for carboxylate oxygens (O_e) and the central μ^3-oxygen, O(1) were refined using separate κ-parameter sets. A set of constraints was introduced to make the net charge on all Cl-atoms equal. In the final refinement, both structural and electronic parameters were varied simultaneously, a total of 988 parameters. Hirshfelds rigid bond[21] test was fulfilled satisfactorily, with a mean value of Δ_{A-B} of 9.8 pm^2. This further confirms that the structure is valence trapped at 100 K.[6] A plot of the residual density in the central Fe_3O-moiety shows no significant features (see Supporting Information).

2. This structure was solved using direct methods.[13] It consists of a $[Fe_3^{III}O]^{7+}$-core with chloroacetate groups bridging the Fe-atoms. Furthermore, two Fe atoms are coordinated in the terminal position by water molecules, whereas the last Fe is bonded to a η^1-chloroacetate group. One statically disordered solvent molecule of water was located in the structure, with the oxygen positions of the two disordered molecules less than 2 Å apart. The disorder was modeled as one water molecule distributed over two positions (88%, 12%) with the major part refined anisotropically. One hydrogen atom position in this water molecule was refined as common to both entities. The other hydrogen of the minor component was not located. Disorder of the chlorine atoms is more evenly distributed in **2** than in **1**. Four chlorine atoms were disordered over two positions with major occupancies in the range from 89 to 98%, whereas two chlorine positions were modeled with one major site (73−95%) and two minor sites. The major parts of the chlorine atoms were refined with anisotropic displacement parameters. No restrictions were enforced on the C−Cl distances, and the resulting C−Cl bond lengths of the minor components are slightly unphysical. Overall, the refinement is very significantly improved by the introduction of the disorder models for the Cl-atoms, but we are aware that we may not only be modeling static disorder, but also anharmonic motion of the chlorine atoms (hence the slightly unphysical bond lengths). This structural model was the starting model for the refinement of the aspherical charge distributions with program XD.[18] Ionic scattering factors[20] were used for Fe^{3+} and the SDS scattering factor[22] was used for all H. The structural skeleton was kept fixed after an initial high-order refinement (sin $\theta/\lambda > 0.8$ Å^{-1}) and the EDD was described with hexadecapoles on Fe and octupoles on the other non-H atoms. Two different types of H were distinguished (C−*H* and O−*H*) and each hydrogen type was refined with one monopole and one bond directed dipole. The radial distribution of Fe was modified by refinement of κ'- and κ''-parameters constrained to be identical. Release of this constraint leads to divergence. A separate κ-set was given to O(1), on which local mirror symmetry across the Fe_3O plane was imposed. Before the final refinement cycles, the C−H and O−H bond distances were prolonged to the realistic values of 1.095 and 0.967 Å, respectively. In the final refinement, all data were used and both structural and electronic parameters were varied simultaneously. The Hirshfeld rigid bond test showed a successful refinement of atomic motion ($<\Delta_{A-B}> = 8.8$ pm^2).

3. The initial structural model was adopted from results of refinements of the structure at higher temperatures, see ref 6, and the multipolar modeling was performed with program XD.[18] The Fe and μ^3-O atoms were modeled to the hexadecapolar, and the O, N, and C atoms to the octapolar level. Two separate sets consisting of one monopole and one bond directed dipole were assigned to the methyl hydrogens and to the pyridine hydrogens. Third-order Gram−Charlier thermal parameters were used on the Fe atoms. Due to correlation between anharmonic thermal and multipole parameters on the Fe atoms these parameters were refined in separate cycles. The refinements employed Fe^{2+} and Fe^{3+} atomic scattering factors.[20] All hydrogens were given an isotropic thermal motion equal to 1.5(1.2) times the equivalent isotropic motion of the connected *tert*-butyl(pyridine) carbon. The H-atoms were moved to positions giving bond distances equal to average neutron diffraction values in the refined bond directions. Because the synchrotron data were found to be the more accurate, only conventional data missing in the synchrotron data were included in the refinement. Below sin$\theta/\lambda = 0.30$ Å^{-1} the included conventional data constitute 110 out of 1151 reflections in the data set. The final model was found to be statistically unaffected by removal of the conventional data in the refinement.

The acentric space group makes it imperative to carefully examine every step of the refinement procedure. It has been shown that for acentric structures it may be difficult to obtain a reliable least-squares solution, because different physical models equally well describe the observed structure factors.[23] In particular, anharmonic motion can correlate with the odd-order multipoles, because both are mainly contributing to the phase of the structure factor and less to the modulus. Introduction of chemically sensible constraints can assist the refinement in reaching a physically reasonable solution. Extensive testing of chemical constraints on the multipole parameters was therefore carried out, and after each model the standard uncertainties of the refined parameters were evaluated. In the final model, all carbon and hydrogen

(17) Allen, F. H.; Kennard, O.; Watson, D. G.; Brammer, L.; Orpen, A. G.; Taylor, R. J. *J. Chem. Soc., Perkin Trans. 2* **1987**, 1−19.
(18) Koritsanszky, T.; Howard, S. T.; Su, Z.; Mallinson, P. R.; Richter, T.; Hansen, N. K. *XD, Computer Program Package for Multipole Refinement and Analysis of Electron Densities from Diffraction Data*; Freie Universität Berlin; Berlin, Germany, June 1997. The 2002 version of the XD program, which includes relativistic scattering factors, was used for all calculations.
(19) The presence of structural disorder makes multipole modelling challenging. However, in this study the disorder is far from the central Fe_3O region, which is the part of the structure of major interest. Furthermore, a quite convincing disorder model could be established. We therefore believe the present results are reliable. In complex **2**, a disordered solvent water molecule is present besides the disordered chlorine atom. The solvent water molecule is assumed to be neutral in the modeling, and this may also be a limitation in the model.
(20) Clementi, E.; Roetti, C. *Atomic Nucl. Data Tabl.* **1974**, *14*, 177.
(21) Harel, M.; Hirshfeld, F. L. *Acta Crystallogr. Sect. B* **1974**, *31*, 162−172. Hirshfeld, F. L. *Acta Crystallogr. Sect. A* **1976**, *32*, 239−244.
(22) Stewart, R. F.; Davidson, E. R.; Simpson, W. T. *J. Chem. Phys.* **1965**, *42*, 3175−3187.
(23) Haouz, E.; Hansen, N. K.; Le Henaff, C.; Protas, J. *Acta Crystallogr. Sect. A* **1996**, 52, 291−301.

Table 2. Selected Bond Lengths in Å

bond	1	2	3
Fe(1)−O(1)[a]	1.850(1)	1.899(1)	1.833(1)
Fe(2)−O(1)	1.859(1)	1.905(1)	1.872(1)
Fe(3)−O(1)	1.994(1)	1.951(1)	2.014(1)
Fe(1)−O_e[b] bt[c] Fe(2)	2.016(1), 2.037(1)	2.049(2), 2.029(2)	2.057(1), 2.031(1)
Fe(3)	2.024(1), 2.013(1)	2.010(2), 2.014(2)	2.007(1) 2.033(1)
Fe(2)−O_e bt Fe(1)	2.064(1), 2,068(1)	2.017(2), 2.011(2)	2.042(1), 2.076(1)
Fe(3)	2.042(1), 2.072(1)	2.027(2), 2.019(2)	2.034(1), 2.015(1)
Fe(3)−O_e bt Fe(1)	2.086(1), 2.105(1)	2.007(2), 2.049(2)	2.080(1), 2.121(1)
Fe(2)	2.114(1), 2.155(1)	2.015(2), 2.023(2)	2.159(1), 2.081(1)
Fe(1)−L[d]	2.149(1)	2.097(2)	2.238(1)
Fe(2)−L	2.110(1)	2.064(2)	2.223(1)
Fe(3)−L	2.118(1)	1.986(2)	2.216(1)
(C−O_e) at Fe(1) bt Fe(2)	1.261(1), 1.264(1)	1.263(3), 1.254(2)	1.264(2), 1.261(2)
(C−O_e) at Fe(1) bt Fe(3)	1.278(2), 1.267(2)	1.263(2), 1.258(2)	1.277(2), 1.270(2)
(C−O_e) at Fe(2) bt Fe(2)	1.251(1), 1.251(1)	1.251(3), 1.261(2)	1.257(2), 1.268(2)
(C−O_e) at Fe(2) bt Fe(2)	1.269(2), 1.276(2)	1.252(2), 1.258(3)	1.273(2), 1.274(2)
(C−O_e) at Fe(3) bt Fe(2)	1.236(2), 1.244(2)	1.245(2), 1.248(2)	1.247(2), 1.255(2)
(C−O_e) at Fe(3) bt Fe(2)	1.241(2), 1.240(2)	1.256(3), 1.244(3)	1.249(2), 1.257(2)

[a] O(1) is the central μ^3-oxygen. [b] O_e is a carboxylate-oxygen bridge. Ordered according to increasing O_e-label number. [c] Bridging toward. [d] L is the ligand atom bonded to Fe trans to O(1).

atoms in the *tert*-butyls were constrained to have identical population parameters. Noncrystallographic *mm* symmetry was imposed on the pyridine rings, which all were constrained to be identical. The two carboxyl groups between each pair of Fe atoms were constrained to be identical. For the planar Fe_3O core mirror symmetry across the plane was tested. The residuals and the refined density only changes little when imposing the mirror symmetry on O(1). However, for the Fe atoms use of mirror symmetry leads to a considerable degradation of the fit, and this constraint was therefore abandoned.

A comparison of the refined multipolar parameters for all three compounds shows that there is very good correspondence between relevant parameters. A complete list of refined multipolar parameters as well as more details about the data reduction and refinement procedures can be obtained from the Supporting Information.

Theoretical Calculations. A single-point calculation in the experimental geometry of molecule **3** was performed using density functional theory as implemented in Jaguar 4.0 (release 23).[24] Topological analysis of the electron density was performed with the AIMPAC programs.[25] The calculation was done using the B3LYP hybrid method[26] and the Los Alamos[27] LACV3P basis set, which is a triple-ζ basis set that places effective core potentials on the iron centers and uses Pople type 6−311g[28] on all other atoms. Considerable efforts are frequently required to reach convergence for calculations of the electronic wave function for transition metal containing systems. Therefore, to save use of excessive amounts of computer time, the recently developed[29] initial guess methodology based on ligand field theory[30] is applied as implemented in Jaguar. The system contains three iron centers all of which are modeled as high spin, in agreement with the experimental results discussed below. Therefore, **3** has a spin multiplicity of 15 (Fe(1) d^5, Fe(2) d^5, Fe(3) d^6 all high spin) giving rise to a system with numerous open shell orbitals. The unrestricted DFT (UDFT) method has been used extensively to model the electronic properties of similar polynuclear iron complexes[31] as well as complexes containing other transition metals.[32] In this paper, we are interested in the EDD, which is not sensitive to the actual coupling of the individual spins on the iron centers. Therefore, this high spin (ferromagnetic) state is expected to produce a good model for the EDD. The spins may show antiferromagnetic coupling, which is an important feature, but no efforts were undertaken to model such spin states using e.g. the broken symmetry approach developed by Noodleman et al.[33]

Results & Discussion

Structural Analysis. The geometry of the coordination sphere around iron atoms contains much information about the oxidation state of these atoms and the degree of ET in the Fe_3O core. In Table 2, selected bond distances and angles in the three compounds are compiled, observing the convention that Fe(1) has the shortest Fe−O(1) distance and Fe(3) the longest, i.e., Fe(1) and Fe(2) are trivalent, and Fe(3) is divalent in the electronically trapped state of the MV compounds. In compound **1**, like in compound **3**, it is Fe(1), which is not involved in the temperature dependent ET (checked by comparison with the room temperature structure). Only slight differences are found in the Fe^{III}−O(1) bond lengths. However, the trans bond between Fe(1) and the coordinated water is significantly *longer* than for Fe(2), $\Delta d = 0.039(1)$ Å. Thus Fe(1) has a larger *trans*-effect than Fe(2) from O(1), and Fe(1)−O(1) appears to be a stronger interaction than Fe(2)−O(1). For Fe(3), the bond distances are as expected for an Fe^{II} atom and correspondingly much longer than for Fe(1) and Fe(2). The average equatorial bond length (Fe−O_e) is shorter for Fe(1) than for Fe(2) despite the fact that the two atoms formally both are Fe^{III} at temperatures below 120 K.[5f] The differences in the Fe−O_e bonds are also reflected in the delocalization of the carboxylate groups, i.e., the asymmetry in C−O bond lengths in the bridging chloroacetates. In the four bridges from either Fe(1) or Fe(2) to Fe(3),

(24) Jaguar 4.0: Schrödinger Inc, Portland, OR, 2000.
(25) Biegler-König, F. W.; Bader, R. F. W.; Tang, T.-H. *J. Comput. Chem.* **1982**, *3*, 317−328.
(26) (a) Becke, A. D. *J. Chem. Phys.* **1993**, *98*, 5648−5652. (b) Becke, A. D. *Phys. Rev. A* **1988**, *38*, 3098−3100. (c) Lee, C. T.; Yang, W. T.; Parr, R. G. *Phys. Rev. B* **1988**, *37*, 785−789.
(27) (a) Hay, P. J.; Wadt, W. R. *J. Chem. Phys.* **1985**, *82*, 270−283. (b) Wadt, W. R.; Hay, P. J. *J. Chem. Phys.* **1985**, *82*, 284−298. (c) Hay, P. J.; Wadt, W. R. *J. Chem. Phys.* **1985**, *82*, 299−310.
(28) (a) Krishnan, R.; Binkley, J. S.; Seeger, R.; Pople, J. A. *J. Chem. Phys.* **1980**, *72*, 650−654. (b) McLean, A. D.; Chandler, G. S.; *J. Chem. Phys.* **1980**, *72*, 5639−5648.
(29) Vacek, G.; Perry, J. K.; Langlois, J.-M. *Chem. Phys. Lett.* **1999**, *310*, 189−194.
(30) Pietro, W. J.; Levi, B. A.; Hehre, W. J.; Stewart, R. F. *Inorg. Chem.* **1980**, *19*, 2225−2229.
(31) See e.g., (a) Siegbahn, P. E. M.; Blomberg, M. R. A. *Chem. Rev.* **2000**, *100*, 421−438. (b) Dunietz, B. D.; Beachy, M. D.; Cao, Y.; Whittington, D. A.; Lippard, S. J.; Friesner, R. A. *J. Am. Chem. Soc.* **2000**, *122*, 2828−2839. (c) Siegbahn, P. E. M. *Inorg. Chem.* **1999**, *38*, 2880−2889. (d) Yoshizawa, K.; Yumura, T. *Chem. Eur. J.* **2003**, *9*, 2347−2358.
(32) See e.g. Zhao, X. G.; Richardson, W. H.; Chen, J. L.; Li, J.; Noodleman, L.; Tsai, H. L.; Hendrickson, D. N. *Inorg. Chem.* **1997**, *36*, 1198−1217.
(33) Noodleman, L.; Deng, C. Y.; Case, D. A.; Mouesca, J.-M. *Coord. Chem. Rev.* **1995**, *144*, 199−244.

d(C−O) is clearly shorter for the bond involving the oxygen coordinated to Fe(3), <d(C−O_e) at Fe(3)> = 1.240(3) Å, compared with <d(C−O_e) at Fe(1,2)> = 1.268(7) Å. In the two bridges between Fe(1) and Fe(2), the asymmetry in d(C−O_e) is less pronounced but still significant, with the oxygens coordinated to Fe(1) being slightly longer. This again indicates that the two Fe^{III} atoms are slightly different (Fe(1) has slightly higher valence). The octahedral coordination around the Fe atoms is not ideal, and the equatorial ligands are displaced outward away from O(1) ($\angle$(O(1)−Fe(1)−O_e)$_{av}$ = 97(1)°, $\angle$(O(1)−Fe(2)−O_e)$_{av}$ = 97(1)° and $\angle$(O(1)−Fe(3)−O_e)$_{av}$ = 94(3)°).

In the structure of **2**, the three Fe atoms are formally identical Fe^{III} atoms, even though a significant difference is introduced with the exchange of a water ligand on Fe(3) with a monodentate chloroacetate. This results in a significant increase in d(Fe(3)−O(1)). For the two other Fe atoms, d(Fe−O(1)) is very close to 1.900 Å, which is similar to Fe−(μ^3-O) bond lengths in other oxidized Fe_3O compounds ($[Fe_3O]^{7+}$-moieties).[34] The different axial ligand to Fe(3) has no effect on <d(Fe−O_e)>, which are 2.026(17) Å, 2.019(7) Å and 2.024(18) Å, respectively, for Fe(1), Fe(2), and Fe(3). These values resemble the value for Fe(1) in **1** (the valence trapped Fe^{III}). A slight asymmetry is found in the C−O distances in the carboxylate bridges to Fe(3). The shorter C−O bond is for the oxygen coordinated to Fe(3), <d(C−O) at Fe(3)> = 1.248(5) Å, indicating that Fe(1) (<d(C−O) at Fe(1)> = 1.260(4) Å) and Fe(2) (<d(C−O) at Fe(2)> = 1.256(5) Å) have a slightly higher valence than Fe(3).

There is a distinct difference in Fe^{III}−O(1) bond lengths between MV and oxidized trinuclear iron complexes (Δd = 0.05−0.10 Å). To comply with the 18-electron rule in the MV TOCIs, the trivalent iron needs a donation of 13 electrons. Eight electrons come from the carboxylate-bridges, two from the terminal ligand, and three from O(1). The divalent iron only needs two electrons from O(1), such that the necessary total electron donation from O(1) to the three Fe atoms is eight, and the number of electrons in the Fe^{III}−O(1) bonds is three, compared with only two in the Fe^{II}−O(1) bond. The situation is different in the oxidized TOCIs, where the three trivalent iron atoms need a total donation of nine electrons from O(1), but will share the eight available, such that the number of electrons in each Fe^{III}−O(1) bond has decreased from three to 8/3 in the MV TOCIs. This corresponds well with the observation that the Fe^{III}−O(1) bond lengths in **2** have increased by ca. 1/3 of the difference between Fe^{III}−O(1) and Fe^{II}−O(1) in the MV TOCI, i.e., 1/3 × (2.0−1.85 Å) = 0.05 Å.

In compound **3** we find that the two Fe^{III}−O(1) bond lengths are slightly different, and that the shorter bond involves Fe(1), which maintains its formal valence of +3 below room temperature. A slight *trans*-effect is observed in the Fe−N bonds, because Fe(1)−N(1) is longer than Fe(2)−N(2). The equatorial Fe−O_e bonds do not provide significant distinction between the oxidation states of Fe(1) and Fe(2) (<d(Fe−O_e)> = 2.03(2) Å, <d(Fe−O_e)> = 2.04(2) Å). As for **1** the C−O bond distances in the pivalate bridges between iron atoms with different valence states reveal a clear partial electronic localization, with one short and one long C−O bond, the longer C−O bond to the oxygen that coordinates to the higher valent iron, see Table 2. The bridges between Fe(1) and Fe(2) show expectedly less localization.

Electron Density Distributions. In discussion of the EDDs, we first compare **1** and **2**, which are structurally very similar. We will concentrate on the central Fe_3O core because this is the region of ET. Density maps of some ligand groups can be found in the Supporting Information. The monopolar values may be taken as crude estimates of atomic charge, q.[8] The charges on the Fe^{III} atoms are very similar in **1** ($q(Fe^{III})_{ave}$ = +1.45(7) e) and **2** ($q(Fe^{III})_{ave}$ = +1.43(1) e), whereas the charge on Fe^{II} in **1** is lower ($q(Fe^{II})$ = +0.72(3) e). The radial κ-parameters for Fe are 0.911(3) in **1** and 0.933(3) in **2**. The negative charge ($q(O_e)$) on the equatorial oxygens in the carboxylate bridges average 0.45(9) in **1** and 0.55(12) in **2**. For three of the four bridges between Fe^{II} and Fe^{III} in **1** there is good correlation between longer C−O bonds and higher atomic charge of O. The radial κ-parameters for O_e show good correspondence (0.987(1) in **1** versus 0.990(2) in **2**). The largest discrepancy between the MV and the oxidized system is found to involve the central O(1). The net charge on O(1) in **1** is q(O(1)) = −1.02(4) (κ = 0.961(4)) and it is q(O(1)) = −1.38(5) (κ = 0.933(4)) in **2**.

In Figure 2 the difference between the static model density and the density of a superposition of neutral spherical atoms is plotted in the Fe_3O planes (static deformation density maps). A strong deviation from 3-fold symmetry is observed for **1** (Figure 2a), whereas such noncrystallographic symmetry is almost present for **2** (Figure 2b). Deformation density maps in planes perpendicular to the Fe_3O planes, and containing one of the Fe−O(1) bonds are shown in Figures 3 and 4. Figures 3a-c show that in **1** there is excess density above and below the Fe_3O plane in the Fe(1)−O(1) bond on both the Fe(1) and the O(1) site (π-type interaction, Figure 3a), contrary to the Fe(2)−O(1) and Fe(3)−O(1) bonds where the density is concentrated in the plane (σ-type interaction, Figures 3b−c). In striking contrast to the MV complex **1**, the oxidized complex **2** exhibits three almost identical Fe−(μ^3-O) interactions, which all have in-plane σ-donation from the central O(1), see Figures 4a-c.

We now turn our attention to the MV complex **3**, which has totally different equatorial and axial ligands compared with **1** and **2**. In **3**, the differences in the atomic charges estimated from the monopole populations are not so distinct between Fe^{III} ($q(Fe^{III})_{av}$ = +1.82(4)e) and Fe^{II} ($q(Fe^{II})$ = +1.47(6)e). The static deformation density in the Fe_3O plane is shown in Figure 2c and perpendicular Fe−(μ^3-O) bonding planes are shown in Figure 5a-c.

As for **1** a clear difference is observed in the bonding to O(1) for the Fe^{III} sites compared with the Fe^{II} site (Fe(3)), Figure 2c. Another crucial feature is seen in Figure 5b. As was also found in the MV complex **1**, the central oxygen is again showing an sp^3-like electron distribution. In **3**, as in **1** and **2**, the Fe_3O moiety is completely planar, and the presence of four valence shell charge concentrations (VSCC, see topological analysis below) arranged in a distorted tetrahedral fashion is therefore surprising. Because this feature is observed in the two very different MV trinuclear complexes **1** and **3**, but not in the oxidized system (**2**), there is strong indication that it is a "fingerprint" of the mixed valence state in trinuclear carboxylates. Because all

(34) (a) Anson, C. E.; Bourke, J. P.; Cannon, R. D.; Jayasooriya, U. A.; Molinier, M.; Powell, A. K. *Inorg. Chem.* **1997**, *36*, 1265−1267, (b) Tong, M.-L.; Chen, X.-M.; Sun, Z.-M.; Hendrickson, D. N. *Transition Metal Chemistry* **2001**, *26*, 195−197, (c) Christensen, K. E. *Master thesis* **2001**, Department of Chemistry, University of Aarhus, Denmark.

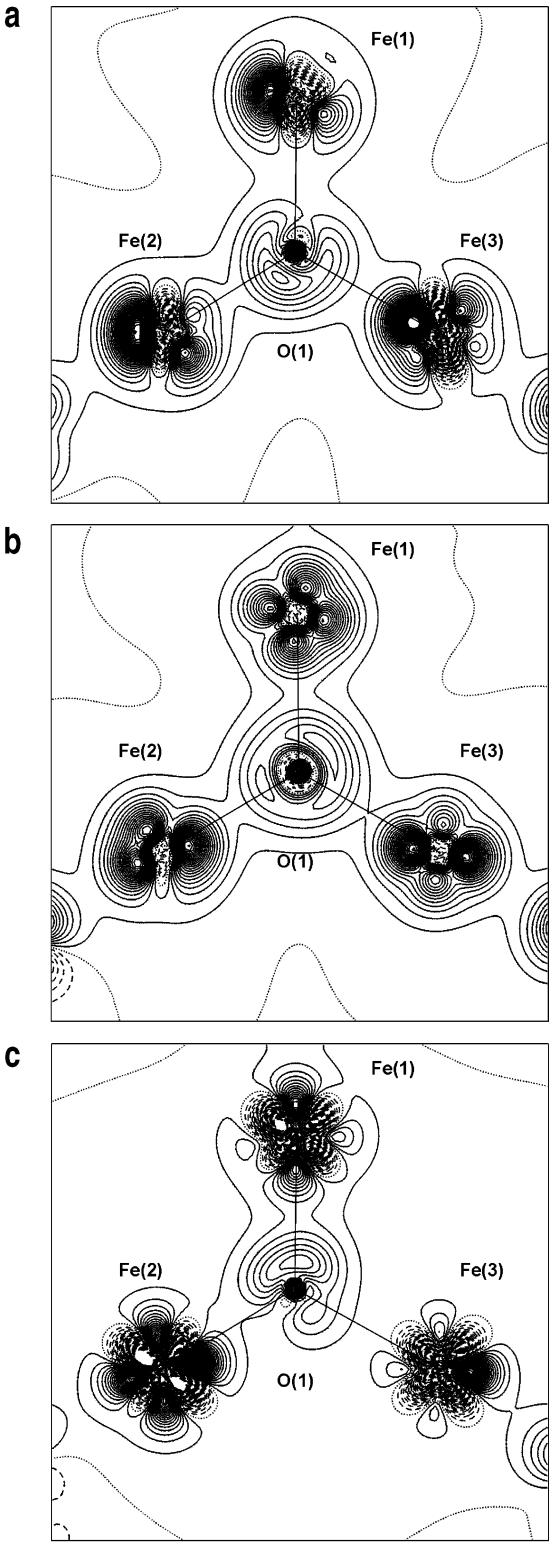

Figure 2. Static deformation density maps in the Fe_3O planes of **1** (a), **2** (b), and **3** (c). Contours at ± 0.1 eÅ^{-3}. Solid lines are positive contours, dashed lines are negative.

ligands (except O(1)) are very different in **1** and **3**, the details of the deformation densities in the Fe_3O cores may differ substantially. Further analysis of density features is carried out below through orbital population and topological analysis.

Orbital Population Analysis. In Table 3 d-orbital populations of the iron atoms are listed as calculated from the refined multipole coefficients.[35] For the description of the d-orbitals

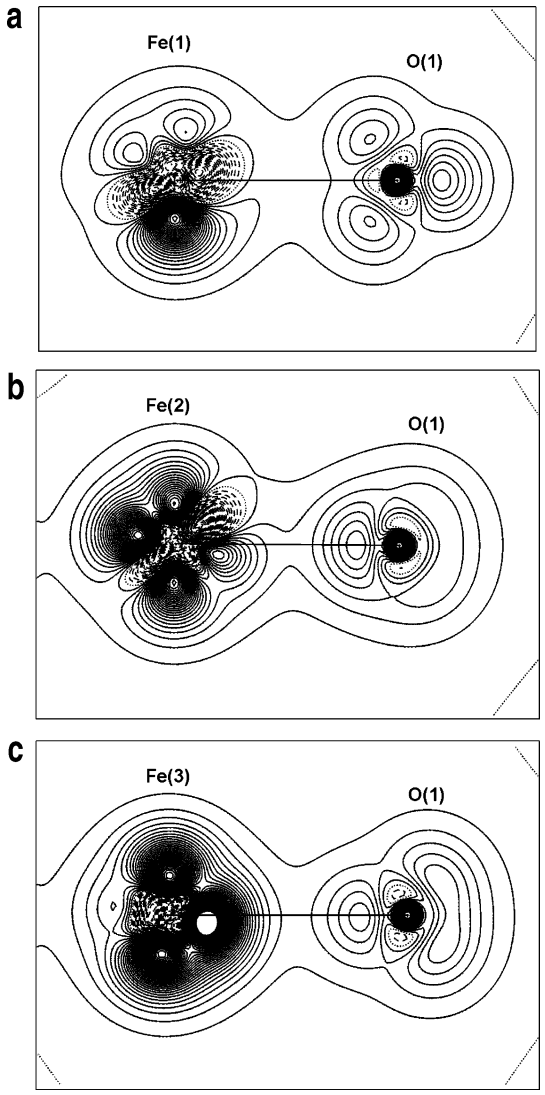

Figure 3. Static deformation density maps in the bonding planes perpendicular to the Fe_3O plane in **1**, containing the Fe−O(1) bonds. Contours as in Figure 2.

the *z*-axis is chosen along the Fe−O(1) direction. The *y* axis points between the equatorial ligands perpendicular to the Fe_3O-plane. Thus, $d(z^2)$ and $d(xy)$ points toward the ligands and are destabilized, whereas $d(xz)$, $d(yz)$ and $d(x^2-y^2)$ are stabilized in the octahedral field. The first overall observation one can make is that all d orbitals are occupied on all the iron atoms. This shows that the experimental EDD is able to distinguish between high and low spin configurations of the Fe atoms, and in these three compounds all metal atoms are high spin.

As for the deformation density analysis we start by comparing the structurally similar compounds **1** and **2**. In the oxidized complex **2** it is striking to see how similar the d-orbital populations are for all the Fe atoms. It should be stressed that this is not a result of "rigidity" in the multipole model, and that the Fe electron parameters have been refined freely without constraints. In the MV complex **1**, there is approximately 0.6 electrons more in the stabilized orbitals on Fe(3) than on Fe(1) and Fe(2), which represents the extra electron density on the Fe^{II} atom relative to the Fe^{III} sites. The extra electron density

(35) Holladay, A.; Leung, P. C.; Coppens, P. *Acta Crystallogr. Sect. A* **1983**, *39*, 377−387.

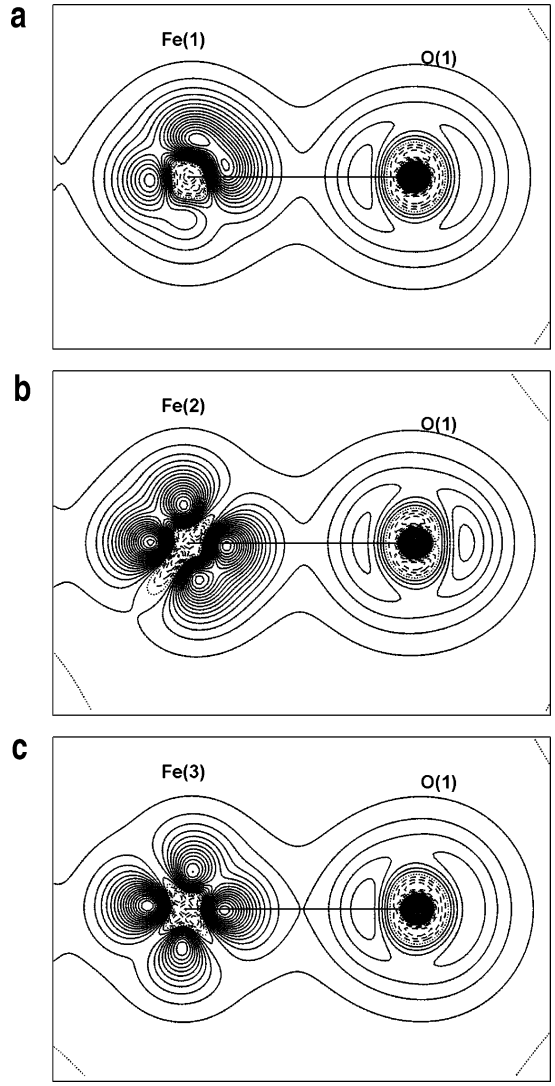

Figure 4. Static deformation density maps in the bonding planes perpendicular to the Fe_3O plane in **2**, containing the Fe−O(1) bonds. Contours as in Figure 2.

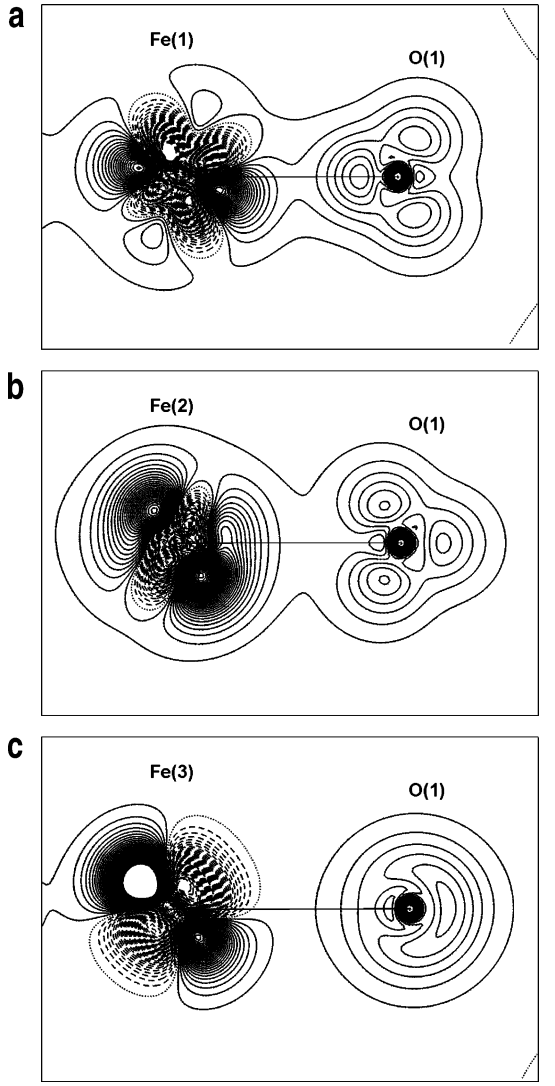

Figure 5. Static deformation density maps in the bonding planes perpendicular to the Fe_3O plane in **3**, containing the Fe−O(1) bonds. Contours as in Figure 2.

on Fe(3) is primarily found in the *d*(*yz*) orbital. Because the two other stabilized orbitals (*d*(*xz*) and $d(x^2-y^2)$) have similar populations for the Fe^{II} site (Fe(3)) and the Fe^{III} sites (Fe(1) and Fe(2)) it appears that the ET in **1** primarily involves transfer of electron density from the *d*(*yz*) orbital on Fe(3) to the *d*(*yz*) orbital on the redox active Fe^{III} site, which in **1** is Fe(2). Another significant difference in the orbital populations of the Fe^{II} and Fe^{III} sites in **1** is the *d*(*xy*) orbital, which accepts σ-donation from the equatorial carboxylate ligands. The σ-donation is larger to the Fe^{III} sites than to the Fe^{II} site (Fe(3)), and this suggests that the population in the stabilized d(yz) orbital on the Fe^{II} site correlates with the d(xy) population, i.e., the σ-donation from the equatorial ligands.

The considerable interaction of the Fe^{III} sites with the equatorial ligands, and the sensitivity of this interaction to the presence of the "extra" d-electron in *d*(*yz*) makes it understandable that changes in the equatorial coordination can significantly influence the ET process. In our multi-temperature crystallographic study of **3** it was found that the onset of disorder in the equatorial ligands correlated strongly with changes in the ET process, and it appeared to be an important factor for selecting which of the two Fe^{III} sites that becomes valence trapped.[6] If an Fe^{III} site has a very strong interaction with the equatorial ligands, then it will require relatively more reorganization of electronic charge upon ET, because it appears that

Table 3. Relative (first line, in %) and Absolute (second line, in electrons) Iron d-orbital Populations

	1			**2**			**3**		
orbital	Fe(1)	Fe(2)	Fe(3)	Fe(1)	Fe(2)	Fe(3)	Fe(1)	Fe(2)	Fe(3)
$d(z^2)$	16.9	21.5	23.5	20.8	22.3	21.8	16.2	21.7	19.0
	1.10	1.42	1.71	1.36	1.47	1.43	1.42	1.34	1.24
d(*xy*)	23.5	21.8	15.8	21.1	20.7	21.3	30.0	19.0	19.2
	1.53	1.44	1.15	1.38	1.36	1.40	1.87	1.17	1.25
Σ destabil.	40.4	43.3	39.3	41.8	43.0	43.1	52.8	40.7	38.2
	2.63	2.86	2.86	2.74	2.83	2.83	3.29	2.51	2.49
d(*xz*)	19.0	18.2	15.5	18.9	19.0	20.2	14.4	17.5	19.8
	1.24	1.20	1.13	1.24	1.25	1.33	0.90	1.08	1.29
$d(x^2-y^2)$	23.0	21.8	23.1	20.3	19.9	19.0	15.7	17.5	17.8
	1.50	1.44	1.68	1.33	1.31	1.25	0.98	1.08	1.16
d(*yz*)	17.5	16.7	22.1	18.9	18.1	17.7	17.0	24.3	24.2
	1.14	1.10	1.61	1.24	1.19	1.16	1.06	1.50	1.58
Σ stabil.	59.6	56.7	60.7	58.2	57.0	56.9	47.2	59.3	61.7
	3.88	3.74	4.42	3.81	3.75	3.74	2.94	3.66	4.03

All absolute values have an estimated standard uncertainty of 0.05 e. The *z*-axis is directed against O(1), *x*- and *y*-axes points between the equatorial ligands, with *y* perpendicular to the Fe_3O-plane.

the $d(xy)$ orbital becomes depleted when d(yz) becomes filled. A very significant difference between the Fe^{III} sites is the bonding to the central O(1). Fe(1) interacts with two VSCCs on O(1) above and below the Fe_3O plane, whereas Fe(2) is involved in normal σ-type interaction with an oxygen lone pair. The π-type interaction for Fe(1) potentially could result in a large difference in the value of the $d(yz)$ orbital for Fe(1) compared with Fe(2) due to π-interaction, but this is not observed. On the other hand Fe(1) has a lower $d(z^2)$ population than Fe(2), which indicates a smaller σ-type interaction for Fe(1) with the axial ligands (see also Table 2, d(Fe(1)−L) > d(Fe(2)−L)).

The d-orbital populations on the iron centers of **3** provide interesting new insight. As in **1**, the extra d-electron density on the Fe^{II} site is again primarily found in the $d(yz)$ orbital. However, contrary to what is observed in **1**, strong π-interaction with O(1) is observed for the valence active Fe(2) site. This π-interaction is seen as a high value for the $d(yz)$ orbital on Fe(2) comparable even with Fe(3) (the Fe^{II} site). In correspondence with the observations for **1** and **2** the presence of a large amount of d(yz) electron density correlates with a decrease in the σ-donation from the equatorial ligands to Fe(2) (and Fe(3)). When comparing the three complexes the lower $d(x^2-y^2)$ values on all irons in **3** compared with **1** and **2** also are noteworthy. We do not yet have a good explanation for this difference.

A number of studies have developed first-order models for the potential energy surface of trinuclear carboxylates.[36] In these models, there are three minima on the potential energy surface corresponding to the situation where the extra d electron is placed at each of the three metal sites. The ET takes place via vibronic coupling, and it is believed that it is especially an asymmetric bond stretch mode of the Fe_3O core, which is active in the ET process. This vibrational mode corresponds to movement of one iron toward the central oxygen along the bond direction (z axis in our coordinate definitions), whereas another iron is moved outward away from the central oxygen along its bond direction. The orbital analysis presented above support that this vibrational mode could be important for the ET. The $d(yz)$, $d(xz)$ and $d(z^2)$ orbital energies are expected to be strongly influenced by the active vibration along the axial bond directions. However, because the $d(z^2)$ orbital is destabilized in an octahedral field, it is the $d(yz)$ and $d(xz)$ orbitals which contain the extra electron density. Both orbitals have π symmetry with respect to bonding to O(1), and thus, the orbital interaction involving $d(yz)$ and $d(xz)$ will be particularly sensitive to the nuclear distance between iron and oxygen.

Topological Analysis. Regions of electron concentration and depletion can be visualized through the scalar function $\nabla^2\rho$ (the Laplacian) calculated on the basis of parameters determined in the multipole analysis of the observed structure factors. Minima in this function correspond to local charge concentrations, and Bader and co-workers have linked such concentrations in the valence shell (Valence Shell Charge Concentrations, VSCC) to the existence of electron pairs.[7] The charge accumulations seen in the deformation densities (Figures 3−5) are reproduced in the Laplacian distributions. Figure 6 shows the Laplacian in the Fe_3O plane, whereas Figures 7a−c show the bonding planes perpendicular to the Fe_3O plane for compound **3**. Laplacian plots of compounds **1** and **2** are included in the Supporting Information. In **1** and **3** the central O(1) has four tetrahedrally distributed VSCCs (average angles between VSCCs are 108.8° and 109.5° respectively), whereas in the oxidized complex **2** they are distributed in a trigonal fashion in the Fe_3O plane (average angle 118°). Again it must be noted that the sp^3-like EDDs on the central oxygen of **1** and **3** are quite surprising given the fact that the Fe_3O cores in all the complexes are completely planar. Thus, these electronic features on O(1) would not be deduced from analysis of the molecular structures (bond lengths and angles).

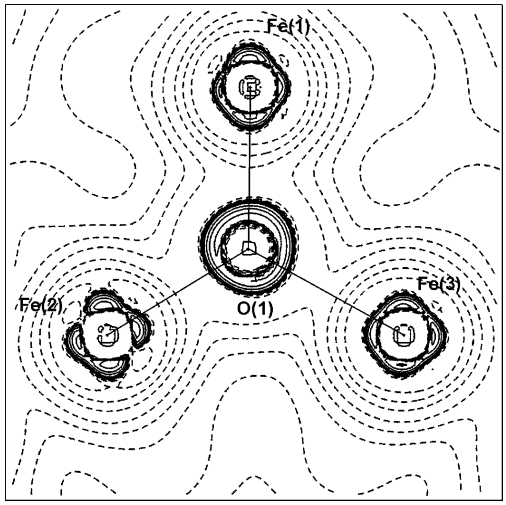

Figure 6. Experimental Laplacian map in the Fe_3O plane of **3**. Contours at ± 2, 4, 8×10^n eÅ^{-5}, $n = -3,-2,-1,0,1,2$. Solid lines are negative contours, dashed lines are positive.

In Figures 8 and 9 theoretical Laplacian maps corresponding to Figures 6 and 7 for the experimental density are shown for **3**. There is quite good correspondence between experiment and theory in the features around the iron atoms, but the central oxygen shows discrepancies. On the iron sites there is a slight tilt of the VSCCs in the experimental density, which is not present in the theoretical density. On O(1) the theoretical density is lacking the sp^3-like distribution of VSCCs observed experimentally. In the Fe(2)−O(1) bond direction oxygen VSCCs are observed above and below the plane in the experiment, whereas the theoretical density has an sp^2-like distribution of the VSCCs. As noted above the sp^3-like distribution of VSCCs appear to be a fingerprint for the mixed valence state in trinuclear carboxylates. Overall, the comparison shows that the experimental density is able to differentiate between fine density features, and thereby validate and constrain detailed theoretical calculations.

We have performed Bader topological analysis[7] of the three EDDs to further understand the bonding in the central Fe_3O regions. Table 4 lists topological parameters at the bond critical points (bcp) for the iron to ligand bonds.

We first look at the oxidized complex **2**. It is remarkable how similar the topological indices are for the different types of Fe^{III}−ligand bonds. It should again be stressed that this is entirely a product of the data, and that it has not been enforced by the model. In the equatorial plane, where the ligands are identical, the topological properties are identical within the standard uncertainty, but for the terminal ligands, L, small

(36) (a) Kambara, T.; Hendrickson, D. N.; Sorai, M.; Oh, S. M. *J. Chem. Phys.* **1986**, *85*, 2895−2909. (b) Cannon, R. D.; Montri, L.; Brown, D. B.; Marshall, K. M.; Elliott, C. M. *J. Am. Chem. Soc.* **1984**, *106*, 2591−2594.

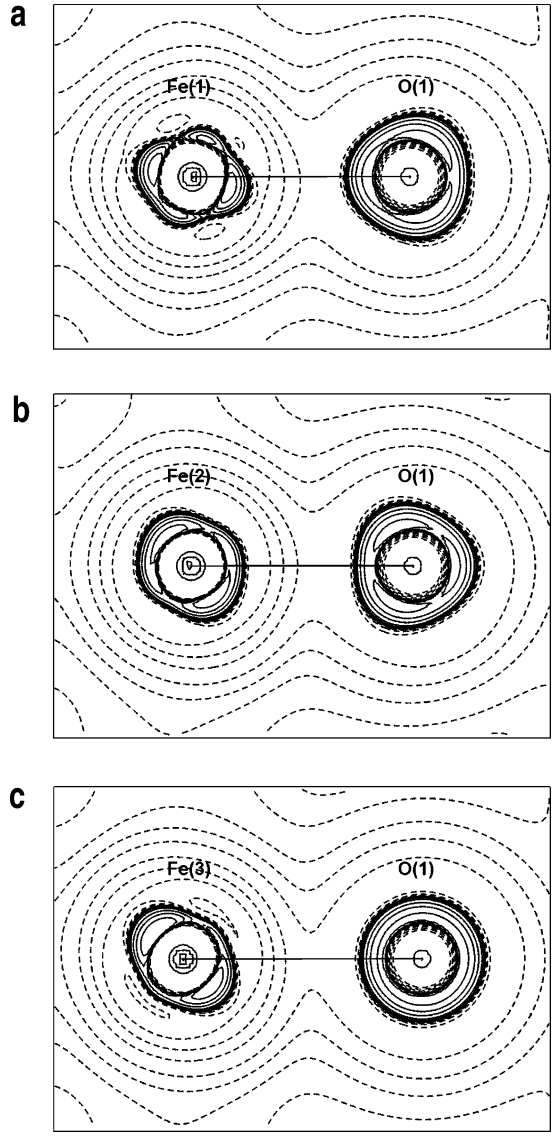

Figure 7. Experimental Laplacian maps in the bonding planes perpendicular to the Fe_3O plane in **3**. Contours at ±2, 4, 8 × 10^n eÅ^{-5}, $n = -3,-2,-1,0,1,2$. Solid lines are negative contours, dashed lines are positive.

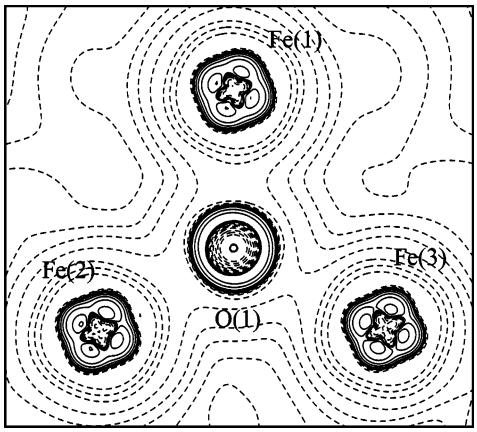

Figure 8. Theoretical Laplacian maps in the Fe_3O plane of **3**. Contours at ±2, 4, 8 × 10^n eÅ^{-5}, $n = -3,-2,-1,0,1,2$. Solid lines are negative contours, dashed lines are positive.

differences are observed between the water and the chloroacetate ligands. The terminal ligand to Fe(3), chloroacetate, is a stronger ligand than water, and thus Fe(3)−L has a slightly larger ρ_{bcp}

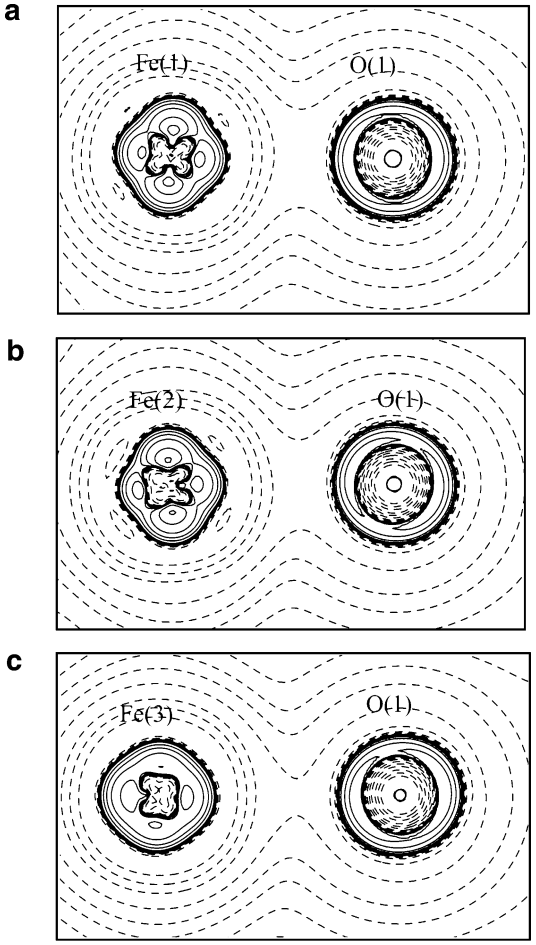

Figure 9. Theoretical Laplacian maps in the bonding planes perpendicular to the Fe_3O plane in **3**, containing the Fe−O(1) bonds. Contours at ±2, 4, 8 × 10^n eÅ^{-5}, $n = -3,-2,-1,0,1,2$. Solid lines are negative contours, dashed lines are positive.

than Fe(1) and Fe(2) which have terminal water ligands. Similarly, both the ionic ($\nabla^2\rho$, G/ρ larger) and covalent (V and H more negative) bonding contributions are slightly increased. The cloroacetate ligand gives a small trans effect on the Fe(3)−O(1) bond observable as a relative bond length increase, but also in the topological parameters, i.e., lower absolute values of ρ_{bcp}, $\nabla^2\rho$, G/ρ, V and H than for Fe(1) and Fe(2). Bigger differences in the bonds are observed in the MV complexes **1** and **3**. In the equatorial plane the Fe^{II} sites have weaker $Fe-O_e$ bonds than the Fe^{III} sites as seen in the covalent contributions to the bonding (ρ_{bcp} is reduced and V is increased). The reduced covalent contribution to the $Fe^{II}-O_e$ bonding was also observed in the orbital analysis above (low d(xy) population). Overall, the topological analysis provides additional information especially about the ionic contributions to the different bonds, which are not reflected in the orbital populations discussed above.

For predominantly electrostatic hydrogen bonds topological measures have been correlated with bonding energies,[38] but such correlations have not yet been established for more complex chemical bonds. Therefore, it is not possible to relate bonding energies to the differences in properties among the Fe sites. In Figure 10 the Laplacian is plotted against the Fe−O bond

(37) Abramov, Y. *Acta Crystallogr. Sect. A* **1997**, *53*, 264−272.
(38) (a) Espinosa, E.; Lecomte, C.; Molins, E. *Chem. Phys. Lett.* **1999**, *300*, 745−748, (b) Espinosa, E.; Alkorta, I.; Elguero, J.; Molins, E. *J. Chem. Phys.* **2002**, *117*, 5529−5542.

Table 4. Topological Measures in the Bond Critical Points (bcp) of the Central Fe_3O Moieties in 1−3

bond	ρ_{bcp} (eÅ^{-3})	$\nabla^2\rho_{bcp}$ (eÅ^{-5})	ϵ	d_{1-bcp} (Å)	d_{2-bcp} (Å)	G/ρ[37]	V	H
				1				
Fe(1)−O(1)	0.75(1)	15.77(3)	0.06	0.947	0.903	1.64	−1.37	−0.13
Fe(2)−O(1)	0.81(1)	16.70(3)	0.06	0.946	0.913	1.66	−1.52	−0.17
Fe(3)−O(1)	0.60(1)	12.58(2)	0.03	1.025	0.969	1.55	−0.97	−0.05
$(Fe(1)-O_e)_{av}$	0.50(2)	10.9(7)	0.07(3)	1.024	0.999	1.53(4)	−0.76(5)	0.01(1)
$(Fe(2)-O_e)_{av}$	0.46(3)	9.8(5)	0.04(3)	1.039	1.022	1.47(1)	−0.67(6)	0.01(1)
$(Fe(3)-O_e)_{av}$	0.40(4)	7.9(9)	0.08(3)	1.069	1.047	1.37(5)	−0.53(8)	0.01(1)
Fe(1)−L	0.35(1)	6.95(1)	0.07	1.073	1.076	1.32	−0.45	0.02
Fe(2)−L	0.41(1)	8.46(1)	0.02	1.062	1.049	1.40	−0.57	0.01
Fe(3)−L	0.43(1)	8.65(1)	0.06	1.058	1.060	1.39	−0.60	0.00
				2				
Fe(1)−O(1)	0.75(1)	15.46(3)	0.03	0.962	0.937	1.63	−1.35	−0.14
Fe(2)−O(1)	0.74(1)	15.31(3)	0.02	0.969	0.936	1.62	−1.33	−0.13
Fe(3)−O(1)	0.65(1)	13.45(2)	0.04	0.985	0.966	1.57	−1.11	−0.08
$(Fe(1)-O_e)_{av}$	0.50(3)	10.9(6)	0.04(2)	1.017	1.009	1.53(2)	−0.76(6)	0.01(1)
$(Fe(2)-O_e)_{av}$	0.506(1)	11.1(1)	0.07(3)	1.016	1.003	1.54(1)	−0.78(1)	0.00(1)
$(Fe(3)-O_e)_{av}$	0.51(4)	11.3(10)	0.04(2)	1.018	1.007	1.56(4)	−0.79(9)	0.01(1)
Fe(1)−L	0.41(1)	8.39(2)	0.06	1.052	1.046	1.40	−0.56	0.02
Fe(2)−L	0.48(1)	10.28(2)	0.08	1.031	1.033	1.49	−0.71	0.00
Fe(3)−L	0.55(1)	12.25(2)	0.08	1.007	0.980	1.58	−0.88	−0.01
				3				
Fe(1)−O(1)	0.86(2)	17.97(4)	0.09	0.942	0.892	1.70	−1.67	−0.21
	0.76	10.46	0.03	0.966	0.883	1.25	−1.17	−0.22
Fe(2)−O(1)	0.71(2)	15.53(3)	0.12	0.971	0.901	1.66	−1.27	−0.09
	0.62	11.45	0.07	0.957	0.918	1.51	−1.07	−0.13
Fe(3)−O(1)	0.47(1)	9.92(2)	0.06	1.020	0.995	1.47	−0.69	0.00
	0.46	7.62	0.20	1.012	1.004	1.23	−0.59	−0.03
$(Fe(1)-O_e)_{av}$	0.51(3)	10.8(10)	0.06(3)	1.036	0.997	1.50	−0.78	−0.02
	0.44	8.2	0.07	1.041	0.999	1.31	−0.57	−0.00
$(Fe(2)-O_e)_{av}$	0.48(2)	9.7(6)	0.08(5)	1.031	1.011	1.43	−0.70	−0.01
	0.40	8.2	0.27	1.034	1.016	1.46	−0.56	0.01
$(Fe(3)-O_e)_{av}$	0.37(5)	7.8(14)	0.12(5)	1.064	1.046	1.39	−0.49	0.03
	0.30	5.6	0.26	1.052	1.070	1.20	−0.32	0.03
Fe(1)−L	0.37(1)	6.14(1)	0.06	1.093	1.146	1.19	−0.44	−0.01
	0.36	4.81	0.08	1.103	1.138	0.92	−0.32	0.01
Fe(2)−L	0.33(1)	5.71(1)	0.26	1.110	1.116	1.19	−0.39	0.01
	0.31	5.22	0.10	1.074	1.164	1.16	−0.35	0.01
Fe(3)−L	0.37(1)	6.44(1)	0.10	1.076	1.140	1.23	−0.46	0.00
	0.31	4.34	0.35	1.073	1.164	0.95	−0.29	0.01

ρ is the electron density and $\nabla^2\rho$ the Laplacian. ϵ is the ellipticity in the bond. G, V and H are the kinetic energy density, the potential energy density, and the total energy density respectively (in hartree Å^{-3}). For **3** the second line refers to the theoretical calculation

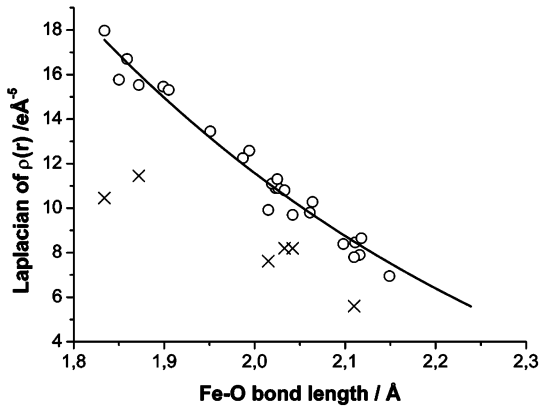

Figure 10. $\nabla^2\rho$ as a function of Fe−O bond length in the three complexes. Circles represent the experimental values for all the complexes, whereas crosses are the theoretical values obtained for **3**. The fitted exponential decay is $\nabla^2\rho = -5.44 + 642*\mathrm{EXP}(-d(\mathrm{Fe-O})/0.55)$ ($R^2 = 0.98$).

lengths in the three complexes. A closer inspection of the values of $\nabla^2\rho$ reveals an exponential decrease with increasing values of the Fe−O bond length. The fit is very good even though the plot is based on results from three completely independent experiments. An exponential decrease is also observed in hydrogen bonds where shorter bonds have larger values of $\nabla^2\rho$.[38] For hydrogen bonds, there is a transition region when going from normal electrostatic hydrogen bonds with positive $\nabla^2\rho$ values to very short covalent hydrogen bonds with negative $\nabla^2\rho$ values.[38] It is an interesting future avenue of research to examine the behavior of very short metal−ligand bonds.

When comparing the experimental and theoretical topological results, the agreement is overall good (Table 1). The density values in the Fe−L bonds are slightly smaller for the theoretical density, but in general the topological measures at the bond critical points are not so sensitive to the differences in the densities. The Laplacian values are systematically smaller for the theoretical density than for the experimental density even though the positions of the critical points agree well.

Conclusion

In the present paper, we have shown that X-ray charge density analysis is a versatile tool, which can improve our understanding of complex molecular systems. Accurate X-ray diffraction data were analyzed for three trinuclear carboxylates of which two are redox active above 120 K (complex **1**) and 35 K (complex **3**), respectively. The fact that experimental EDDs can be obtained even on a 133 atom (542 e$^-$) complex including three open shell iron atoms crystallized in an acentric spacegroup testifies to the significant advances that have occurred with the availability of synchrotron radiation, helium based cooling

devices and accurate area detectors. The MV state of the trinuclear complexes is characterized by having a clear electronic difference between the Fe^{II} site and the two Fe^{III} sites. In the oxidized complex, all Fe^{III} atoms appear very similar. In the MV state the central oxygen has an unexpected hybridization with four VSCCs even though the central Fe_3O core is planar. This indicates that the electronic structure of the central oxygen atom is important for the function of these mixed valence complexes. Orbital population analysis based on the EDDs of the mixed valence versus oxidized complexes revealed some novel insight about intramolecular ET processes in trinuclear complexes. The extra electron density on the Fe^{II} site is distributed primarily in the d(yz) orbital (*z* axis toward O(1), *y* axis perpendicular to the Fe_3O-plane). Upon ET, electron density is moved to the d(yz) orbital of the redox active Fe^{III} site. Presence of extra charge in the d(yz) orbital correlates with a depletion of charge in the equatorial region and a decreased population of the *d*(*xy*) orbital. This suggests that the equatorial ligands have a strong influence on the ET process. Bader topological analysis was used to complement the insights gained from orbital population analysis, and in particular it provided information about the ionic contributions to the transition metal to ligand bonding. An exponential relationship was observed between the Fe−O bond length and the value of $\nabla^2\rho$ at the bond critical point. The comparison between theory and experiment reveal a good agreement, except for the unusual sp^3 distribution on the central oxygen atom. Future X-ray charge density studies of other valence trapped trinuclear complexes also will be very important for designing and fine-tuning the attractive physical and chemical properties of these fascinating molecular systems. Finally, it should be noted that the present information about ET processes in trinuclear oxo-centered iron complexes cannot be deduced from analysis of the molecular structures (i.e., bond lengths and angles). This means that a detailed understanding of redox active centers in biological systems may require structural information beyond bond lengths and angles, which are the typical results of protein crystallographic studies at atomic resolution.

Acknowledgment. We gratefully acknowledge the beam time obtained at beam line X3A1, the National Synchrotron Light Source, Brookhaven National Laboratory, USA. The SUNY X3 beam line at NSLS is supported by the Division of Basic Energy Sciences of the US Department of Energy (DEFG0286ER45231). The Danish Center for Scientific Computing at University of Aarhus is thanked for allocation on the Origin2000 facility for carrying out the theoretical calculations. B.S. thanks the Danish Natural Science Research Council for a Steno grant.

Supporting Information Available: Crystallographic information files, maps of the residual density, and the Laplacian of the electron density. Figure showing the Cl-disorder in **1**. Tables of refined multipolar parameters. This material is available free of charge via the Internet at http://pubs.acs.org.

JA0346072